Ion Cyclotron Resonance Heating with Shifted Separatrix

Ya.I. Kolesnichenko[1], H. Patten[2]‡, V.V. Lutsenko[1], J.P. Graves[2], T.S. Rudenko[1] and JET Contributors*

[1]Institute for Nuclear Research, Prospekt Nauky 47, Kyiv 03028, Ukraine
[2]École Polytechnique Fédérale de Lausanne (EPFL), Swiss Plasma Center (SPC), CH-1015 Lausanne, Switzerland

Abstract. Ion cyclotron resonance heating, which we refer to as ICRH-SS, with the quasilinear separatrix (i.e., the separatrix in the space of quasilinear routes of ion acceleration) located in the region of passing particles is studied. The aim of ICRH-SS is to minimize the fraction of trapped particles (particles with small longitudinal velocities) in the population of fast ions. The basic idea of ICRH-SS – shifting the separatrix to the region of passing particles – was advanced in the paper [*Kolesnichenko et al.*, Nuclear Fusion **57** (2017) 066004]. In this work, new features of ICRH-SS are revealed. The 3-D quasilinear routes of the particle acceleration and effects of Coulomb collisions are studied. A quasilinear equation for distribution function of NBI ions, which is convenient for analysis, is derived. Conditions for quasilinear flux prevailing over collisional flux caused by pitch scattering are obtained. Numerical simulations using the SCENIC package are carried out for a JET plasma with NBI (neutral beam injection) ions that are accelerated by RF field in the core region. A JET pulse designed as a demonstration of the so called "three ions" scheme, which also complies with the criteria of ICRH-SS scheme, was selected. The numerical results show that in the considered example most accelerated ions have larger longitudinal velocities and fast particle orbits are passing during ICRH-SS, whereas, "conventional" ICRH (defined as ICRH with the separatrix in the region of trapped particles) produces accelerated ions with banana orbits. Numerical results also show an increase in fast ion generation and core plasma heating performance for ICRH-SS as compared to the conventional ICRH.

1. Introduction

The Ion Cyclotron Resonance Heating (ICRH) is widely used for plasma heating in tokamaks and stellarators. During ICRH, the energy of generated waves with frequencies close to the ion gyrofrequency or its harmonic are absorbed by resonant ions. This leads to acceleration of these ions and concomitant heating of the plasma due to Coulomb collisions between the accelerated ions and thermal particles. The accelerated ions may

‡ Present address: Department of Statistics, University of Oxford, OX1 3LB Oxford, United Kingdom
* See the author list of "Overview of the JET preparation for Deuterium-Tritium Operation" by E. Joffrin *et al* 2019 *Nucl. Fusion* **59** 112021

increase fusion reactivity and can, in principle, be used to study physics of fast ions in toroidal plasmas. On the other hand, the production of accelerated ions can be a drawback of ICRH. The issue is that the absorbed RF power increases mainly transverse energy of the ions, increasing transverse beta ($\beta_\perp$ is the ratio of the transverse plasma pressure to the magnetic field pressure) and decreasing the ratio of $v_\parallel/v$, where v is the particle velocity and $v_\parallel$ is the velocity along the magnetic field. The increase of $\beta_\perp$ may be unfavourable for plasma equilibrium. The decrease of $v_\parallel/v$ increases the particle orbit width and often leads to transformation of passing particles into trapped ones. The production of trapped energetic ions is a big disadvantage of ICRH for stellarators because the confinement of energetic ions with small $v_\parallel/v$ is a weak point in these machines. The orbits of trapped particles are relatively narrow in large tokamaks and, therefore, the particle confinement is good. Nevertheless, because the orbit width of trapped particles well exceeds that of passing particles, the production of trapped particles broadens the profile of plasma heating by ICRH. Depending on direction of motion of passing particles along the magnetic field, orbits are widened inwards (for co-passing particles, $v_\parallel > 0$) or outwards (for counter-passing particles, $v_\parallel < 0$) when particles become trapped. In the latter case the orbit transformation is detrimental. In the former case, the effect can be positive, unless radial diffusion via random walks of banana orbits is caused by either the discrete nature of the tokamak magnetic field coils [1] or via anomalous diffusion, which will deteriorate the confinement of produced trapped particles. Positive effects take place only when the cyclotron resonance occurs well away from the magnetic axis. In the contrary case, when co-passing particles experience resonance at the magnetic axis, no orbit transformation occurs but the orbit width increases during acceleration.

In connection with this, an idea to minimize the fraction of trapped energetic particles was advanced in reference [2]. A key finding in [2] is that there exists a simple relation between the frequency of a wave generated by the RF-antenna and the on-axis gyrofrequency of fast ions, for which trapped particles are transformed into passing ones during their acceleration, whereas passing particles do not undergo orbit transformation.

To understand the physics underlining this idea, one has to take into account that (i) the particle acceleration during ICRH occurs along characteristics in the space of Constants Of Motion (COM) of a quasilinear (QL) equation for the ion distribution function, (ii) there is a separatrix in this space, (iii) the particles approach the separatrix during acceleration. Usually the separatrix is located in the region of trapped particles, therefore it is natural to refer to this ICRH as "*conventional*" ICRH. Passing particles moving along quasilinear characteristics can then cross the passing-trapped boundary, approaching the separatrix during their acceleration. In this case, passing particles undergo orbit transformation, becoming trapped ones. In order to avoid this, it was proposed in Ref. [2] to move the separatrix to the region of passing particles. We refer to this RF heating as *ICRH with Shifted Separatrix*, or *ICRH-SS*. During ICRH-SS the accelerated passing particles remain passing, whereas trapped particles may cross the passing-trapped boundary and become passing.

Note that conventional ICRH does not necessarily induce passing-trapped conversion: when the acceleration is weak, strongly-passing particles do not reach the separatrix, in which case they remain passing, although their orbit width increases.

Shifting the separatrix to the passing region can be done by increasing the RF-wave frequency (ω) and / or, decreasing the magnetic field strength in comparison to conventional ICRH (for details see section 3). Because of this, cyclotron resonance $\omega = l\omega_B(\mathbf{r})$ [$\omega_B(\mathbf{r})$ is the ion gyrofrequency, $\mathbf{r}$ is a particle radius-vector, l is an integer] on the particle orbit is no longer possible. As a result, particles can be in the resonance with waves only if the frequency Doppler shift is sufficiently large. This means that the ICRH-SS is a particular case of general Doppler-shifted ICRH schemes which were studied for various scenarios in many works, see, e.g. [6, 7], and others.

A distinguished feature of ICRH-SS is that it minimizes the fraction of fast ions with small longitudinal velocities (more exactly: it decreases the pitch parameter $\lambda \equiv \mu\bar{B}/\mathcal{E}$ of accelerated particles, where $\bar{B}$ is the magnetic field at the magnetic axis, $\mathcal{E}$ and μ are the particle energy and magnetic moment). Shifting the separatrix should be consistent with specific experimental conditions, which may restrict changing the magnetic field or the wave frequency. Usual ICRH requirements, such as the fulfillment of the resonance condition for a certain group of ions, proper wave polarization, etc. should be satisfied, of course, too. Resonance interaction of ions and RF-field with frequency close to any harmonic of the ion gyrofrequency always occurs according to the condition

$$\omega_{Dop} = l\omega_B, \tag{1}$$

where $\omega_{Dop} = \omega - k_\parallel v_\parallel$ is the Doppler shifted frequency with $k_\parallel v_\parallel \ll \omega$. Therefore, we establish a "border" between conventional ICRH and ICRH-SS. In tokamaks this border can be given by a certain radius r_{bor} determined by equation $r_{sep} = r_{tp}$, where r_{sep} and r_{tp} are the radii of separatrix and trapped-passing boundary, respectively (see section 2).

In the case of ICRH-SS, equation (1) with given $k_\parallel$ is satisfied provided that $v_\parallel$ is sufficiently large. This implies that normally ICRH-SS is applicable to superthermal ions, such as NBI ions.

A subset of the large variety of ICRH schemes that comply with the ICRH-SS definition are Doppler-shifted ICRH-NBI heating schemes. Aside from ensuring the cyclotron resonance condition is satisfied for a target population - a basic ingredient common to any RF heating scheme - ICRH-SS seeks to modify the quasilinear separatrix configuration space to minimize the trapped and enhance the passing energetic particle fraction, hereby indirectly potentially ensuring more modest particle losses while enhancing the neutron rate. As an illustration for which both experimental data as well as detailed modelling are available, the authors choose to illustrate the wave-particle and particle-particle dynamics underlying ICRH-SS in a dedicated section 5, discussing JET shot #91256. This shot relied on a Doppler-shifted resonance to heat NBI ions on-axis by applying the 3-ion species scheme with the proper RF frequency to a $D - (D_{\mathrm{NBI}}) - H$ plasma [3], the D beam sub-populations with energies close

to the launch energy playing the role of the preferentially heated minority. Key to the 3-ion scheme is to adopt a proper mix of concentrations ensuring the polarisation responsible for ion heating is maximised due to the presence of an ion-ion hybrid layer at the location where the Doppler-shifted cyclotron resonance of the target species lies, this ensuring strong wave absorption. In view of the simultaneous importance of finite orbit width effects, trapping and plasma inhomogeneity aside from the actual wave-particle interaction, a sufficiently sophisticated wave and particle model is required to model the ultimate fate of wave energy. The adopted shot was numerically studied earlier by Patten, in a paper illustrating the intricacies of RF heating both for tokamaks and stellarators [4]. The simulations were made using the SCENIC suite of codes [5] and were validated against experimental diagnostics via the neutron distribution and total neutron count. The differences between the adopted scheme and standard on-axis heating highlighted the importance of actively steering the passing and trapped population fractions when optimising wave heating schemes. This article also aims to extend the research of Patten into the JET simulations presented in [4] to provide a more detailed understanding of the workings of the ICRH-SS scheme than previously shown numerically in [4].

The article attempts to advance theoretical knowledge by extending analysis of reference [2] and making a numerical modelling which demonstrates differences between ICRH and ICRH-SS. Its specific aims are (i) to consider 2-D QL-picture and relevant resonances in more detail, (ii) to take into account 3-D effects in the quasilinear diffusion, (iii) to study the influence of Coulomb collisions, (iv) to consider a particular numerical example of ICRH-SS and conventional ICRH by means of the SCENIC code [5].

The structure of this article is as follows: In section 2 a quasilinear operator in a form convenient for analysis of passing particles is derived, local and global resonances are considered. Quasilinear routes for both passing particles and trapped particles during ICRH-SS in 2-D space (in the plane of the particle energy and pitch parameter) and 3-D space (2-D space supplemented with the canonical angular momentum) are studied in section 3. The influence of Coulomb collisions on NBI ions affected by ICRH-SS are studied in section 4. Numerical simulations aimed to demonstrate differences in the fast ion behaviour during conventional ICRH and ICRH-SS are carried out in section 5. The results obtained are summarized and discussed in section 6.

2. Quasilinear operator and wave-particle resonances

Quasilinear evolution of the particle distribution function implies that COMs vary under the influence of RF field. When the equilibrium magnetic field of a toroidal system is axisymmetric, it is convenient to use the following COMs: the energy, $\mathcal{E}$, the pitch parameter, λ, and the canonical angular momentum, P_φ. They are defined as $\lambda = \mu\bar{B}/\mathcal{E}$, μ the particle magnetic moment, $\bar{B}$ the magnetic field at the magnetic axis, and $P_\varphi = Mv_\parallel R - e\psi_p/c$, with ψ_p the poloidal magnetic flux and R is a distance from the major axis of the torus. The main effect of the RF field during ICRH is the increase

of the particle energy and the change of the particle pitch. The change of P_φ is less important and, therefore, it will be considered later.

When RF frequency is close to a harmonic of the ion gyrofrequency, $l\omega_B$ (l is an integer, $l \sim 1$), the wave-particle interaction is associated mainly with single harmonic. Due to this, routes of quasilinear evolution of the ion distribution function, F, are determined by characteristics of the equation $\hat{\Pi}F = 0$, with $\hat{\Pi}$ an operator which depends on selected l [2]:

$$\hat{\Pi} = \mathcal{E}\frac{\partial}{\partial \mathcal{E}} + (\lambda_l - \lambda)\frac{\partial}{\partial \lambda} = \frac{\partial}{\partial \mathcal{E}}\mathcal{E} + \frac{\partial}{\partial \lambda}(\lambda_l - \lambda), \tag{2}$$

$\lambda_l = l\lambda_*$, $\lambda_* = \bar{\omega}_{Bi}/\omega$, $\bar{\omega}_B = \omega_B(\bar{B})$.

Only resonant particles are affected by the RF field. The resonance equation is

$$\Omega \equiv \omega - l\omega_B(r, \vartheta) - k_\parallel v_\parallel - \mathbf{k}_\perp \cdot \mathbf{v}_D = 0, \tag{3}$$

where $\omega_B(r, \vartheta)$ is the local gyrofrequency, $\mathbf{v}_D$ is the particle drift velocity, $k_\parallel$ and $\mathbf{k}_\perp$ are the longitudinal and transverse wavenumbers, respectively. We will take the gyrofrequency in the form $\omega_B(r, \vartheta) = \bar{\omega}_B(1 - \epsilon \cos\vartheta)$, with ϑ the poloidal angle, $\epsilon = r/R$, r is a radial coordinate (flux coordinates are used). Then equation (3) determines the poloidal angles ϑ_j, with $j = 1, 2$ ($\vartheta_1 = -\vartheta_2$) at a given flux surface where resonance occurs. The drift term can be neglected when $\mathbf{k}_\perp \cdot \mathbf{v}_D \ll \epsilon l \bar{\omega}_B$, which gives the following condition:

$$k_\perp \rho \frac{\rho}{lr} \ll 1, \tag{4}$$

where $\rho = v/\bar{\omega}_B$ is Larmor radius. We assume that this is the case, excluding from consideration resonances close to the magnetic axis where inequality (4) breaks. Taking into account particles with the orbits crossing the axis or passing very near it complicates analysis but does not reveal new physics: quasilinear routes in the COM space do not depend on the orbit shape.

A generic form of the quasilinear operator is

$$Q(F) = \sum_{k,l} \frac{1}{\sqrt{g}} \hat{\Pi} \sqrt{g} D_{k,l} \hat{\Pi} F, \tag{5}$$

where g is determinant of a metric tensor, $D_{k,l}$ is the quasilinear diffusion coefficient. Equation (5) is valid for both passing and trapped particles. However, the diffusion coefficient of trapped particles differs from that of passing ones.

Below we obtain the diffusion coefficient for passing particles. The simplest way to do it is to introduce inhomogeneity of the magnetic field to a QL operator obtained in the homogeneous magnetic field approximation, as suggested by Stix [8].

To follow this way, we proceed from the equation [9]

$$Q(F) = v_\parallel \sum_{k,l} \left[\frac{\partial}{\partial \mathcal{E}} + \frac{l\omega_B}{\omega}\frac{\partial}{\partial \mathcal{E}_\perp}\right] v_\parallel^{-1} D_{kl} \left[\frac{\partial}{\partial \mathcal{E}} + \frac{l\omega_B}{\omega}\frac{\partial}{\partial \mathcal{E}_\perp}\right] F, \tag{6}$$

where

$$D_{kl} = \pi e^2 v_\perp^2 |E_+|^2 \mathcal{I}_l^2 \delta(\Omega), \tag{7}$$

$$\mathcal{I}_l^2 = J_{l-1}^2 \eta_l, \quad \eta_l = \left| 1 + \frac{E_- J_{l+1}}{E_+ J_{l-1}} e^{2i\psi} \right|^2, \tag{8}$$

$\mathcal{E}_\perp$ is the particle energy across the magnetic field, $E_\pm$ are the wave electric field components that rotate in the ion / electron directions, $J_l = J_l(k_\perp v_\perp/\omega_B)$ is Bessel function of l-th order, $\psi = tg^{-1} k_b/k_r$, k_r and k_b are the radial and binormal components of the wavevector. In this equation we neglected the wave component $E_\parallel$ which plays a minor role in the ion-wave interaction through the cyclotron resonance. As in reference [8], we average the diffusion coefficient over a flux surface, taking $\omega_B = \bar{\omega}_B(1 - \epsilon \cos\vartheta)$ and using equation

$$\delta(\Omega) = \sum_{j=1,2} \frac{\delta(\vartheta - \vartheta_j)}{l\bar{\omega}_B \epsilon |\sin\vartheta_j|}. \tag{9}$$

As a result, proceeding to variables $\mathcal{E}$ and λ, we obtain the quasilinear operator for passing particles in tokamaks in the following form:

$$Q(F) = \frac{1}{\sqrt{g}} \hat{\Pi} \sqrt{g} \frac{\mathcal{K} \lambda \mathcal{I}_l^2}{\mathcal{E}} \hat{\Pi} F, \tag{10}$$

where $\hat{\Pi}$ is given by equation (2),

$$\mathcal{K} = \sum_{k,j=1,2} \frac{e^2 |E_+|^2}{M l \bar{\omega}_B \epsilon |\sin\vartheta_j|}, \tag{11}$$

$d^3v = \sum_\sigma d\mathcal{E} d\lambda \sqrt{g}$, $\sqrt{g} = \sqrt{2}\,\pi M^{-3/2} \sqrt{\mathcal{E}/(1-\lambda)}$, ϑ_j are solutions of equation (3), $J_l = J_l(z)$, $z = k_\perp v_\perp/\bar{\omega}_B$, $v_\perp^2 = 2\mathcal{E}\lambda/M$.

Note that the same result can be obtained by means of a more rigorous procedure. To demonstrate it, let us use variables $(\mathcal{E}_\parallel, \mathcal{E}_\perp)$, where $\mathcal{E}_\parallel$ is the particle energy along the magnetic field. Then, neglecting the QL evolution of the distribution function along $\mathcal{E}_\parallel$ and taking $\eta_l = 1$ we reduce equation (10) to

$$Q(F) = \mathcal{K} \frac{\partial}{\partial \mathcal{E}_\perp} \mathcal{E}_\perp J_{l-1}^2 \frac{\partial}{\partial \mathcal{E}_\perp} F. \tag{12}$$

This equation coincides with equation (37) of reference [10], which was obtained from a bounce-averaged quasilinear equation in the limit of overlapped "global" resonances given by

$$\bar{\Omega} - s\omega_b = 0, \tag{13}$$

with

$$\bar{\Omega} = \omega - l\bar{\omega}_B - m\langle\dot{\vartheta}\rangle + n\langle\dot{\varphi}\rangle, \tag{14}$$

where s is an integer, $\langle(...)\rangle$ means bounce / transit averaging, φ is the toroidal angle, "dot" over letters means time derivative, m and n are the poloidal and toroidal wave numbers, respectively [it was assumed that perturbed quantities are proportional to $\exp(-i\omega t + im\vartheta - in\varphi)$].

Global resonances exist for time intervals exceeding the bounce / transit period. Because the quasilinear diffusion coefficient is considerable only when the local resonance

(3) occurs, equation (13) is actually a relationship between ϑ_j and s. For passing particles it reads:

$$s\omega_b + l\bar{\omega}_B\epsilon\cos\vartheta_j = 0. \tag{15}$$

The overlap of bounce / transit resonances represents a factor providing stochasticity and, thus, plasma heating by the RF field.

The factor $\mathcal{K}$ contains a singularity at $\vartheta_j = 0,\ \pi$. Therefore, we transform it to another form. Let us assume that the summation over $\mathbf{k}$ in equation (11) is determined mainly by the antenna power spectrum over k_φ, with $k_\varphi = -n/R$. Then $dk_\parallel = dk_\varphi$, and we can replace $\sum_k(...)$ with $\sum_n(...) = R\int dk_\parallel(...)$. This procedure (replacement of the sum by the integral) is justified provided that the local resonances associated with various mode numbers overlap. We assume that this is the case. Now we take into account that resonance (3) determines a dependence of ϑ_j on $k_\parallel$ for a particle characterized by radial coordinate (r) and longitudinal velocity ($v_\parallel$), which leads to relation

$$\frac{\partial\vartheta_j}{\partial k_\parallel} = -\frac{v_\parallel}{\epsilon l\bar{\omega}_B\sin\vartheta_j}. \tag{16}$$

Then we obtain:

$$\mathcal{K} = e^2R\left[\frac{2}{M\mathcal{E}(1-\lambda)}\right]^{1/2}\sum_{j=1,2}\int d\theta_j|E(\vartheta_j)|^2, \tag{17}$$

where $E(\vartheta_j) = E_+[k(\theta_j)]$, $\lambda < 1$. The integral in this equation vanishes for those ϑ_j for which the resonances with given $\mathcal{E}$, λ, and r are absent and / or the wave amplitudes $E(\vartheta_j)$ are negligible. For instance, when waves with wave numbers in the range $\hat{k}_\parallel \le k_\parallel \le \hat{k}_\parallel + \Delta k$ lead to resonance (3) at $\hat{\vartheta} \le \vartheta \le \hat{\vartheta} + \Delta\vartheta$, equation (16) provides the following relationship between $\Delta\vartheta$ and $\Delta k_\parallel$:

$$\cos(\hat{\vartheta} + \Delta\vartheta) - \cos\hat{\vartheta} = \frac{\rho_\parallel}{\epsilon l}\Delta k_\parallel. \tag{18}$$

In particular, for $\hat{\vartheta} = \pi$, $k_\parallel\rho_\parallel = l\epsilon$, and $k_\parallel = -n/R$ we obtain

$$\Delta\vartheta = \cos^{-1}\left(1 - \frac{\Delta n}{\hat{n}}\right), \tag{19}$$

which yields $\Delta\vartheta = \sqrt{2\Delta n/\hat{n}}$ for $\Delta n/\hat{n} \ll 1$.

Relation (17) for $\mathcal{K}$, in contrast to (11), does not have singularity.

3. Quasilinear routes during ICRH-SS

3.1. Basic idea of ICRH-SS: 2-D analysis

Characteristics of operator (2) are determined by the following equation:

$$\frac{d\mathcal{E}}{\mathcal{E}} = \frac{d\lambda}{\lambda_l - \lambda}. \tag{20}$$

Its solution is

$$\mathcal{E}\left(\lambda_l - \lambda\right) = C_{\mathcal{E}}, \tag{21}$$

where $C_{\mathcal{E}}$ =const, $C_{\mathcal{E}} > 0$ for $\lambda < \lambda_l$ and $C_{\mathcal{E}} < 0$ for $\lambda > \lambda_l$.

It follows from here that there exists a separatrix, λ_l, which separates the regions with $d\lambda/d\mathcal{E} > 0$ and $d\lambda/d\mathcal{E} < 0$. The increase of the particle energy is accompanied by approach of λ to λ_l. During conventional ICRH $\lambda_l > \lambda_{max}^{pas}$, where λ_{max}^{pas} is the upper border of the region of passing particles ($0 \leq \lambda < \lambda_{max}^{pas}$ for passing particles). This explains why passing particles tend to become trapped ones during ICRF.

In contrast to this, following [2] we assume that

$$\lambda_l < \lambda_{max}^{pas}. \tag{22}$$

Due to this choice of λ_l, although the pitch parameter λ of passing particles with $0 < \lambda < \lambda_l$ increases during heating, but, nevertheless, these particles cannot reach the trapped particle region (where $\lambda > \lambda_{max}^{pas}$). The pitch parameters of two groups of particles – the passing particles with $\lambda_l < \lambda < \lambda_{max}^{pas}$ and the trapped particles – decrease during their motion to the separatrix λ_l. Therefore, the marginally passing particles become more passing, but trapped particles undergo orbit transformation and become passing.

For particles with standard (narrow) orbits in tokamaks $\lambda_{max}^{pas} \approx 1 - r/R$, which follows from $v_\parallel = 0$ and, therefore, it does not depend on the sign of $v_\parallel$. This is the case for particles with $\Delta_b < r$, where Δ_b is the orbit width, and r is the average radius of particle location. In the limit case of orbits passing through the magnetic axis, the orbit transformation accompanied with sharp change of the maximum particle displacement from the axis (r_{max}) occurs at the pitch $|\chi(0)| \equiv |v_\parallel(r=0)|/v \sim \hat{s}^{1/3}$ ($\hat{s} = 2q\rho/(\delta_E R)$, with $\rho = v/\omega_B$ and δ_E the plasma cross section elongation), but only for $v_\parallel < 0$, see e.g. [11]. Maximum displacement of co-passing particles is a monotonic function of $\chi(0)$ and is relatively small, $r_{max} \approx \hat{s}^{2/3} R$ at $\chi(0) = 0$, and r_{max} is a decreasing function of $\chi(0)$ in the region $\chi(0) > 0$, so that $r_{max} \sim q\rho$ when $\chi(0) \sim 1$. In comparison to ICRH, ICRH-SS produces particles with smaller λ, which means that $\chi(0)$ is larger and r_{max} is smaller.

Below we assume that orbits are standard. Figure 1 demonstrates the difference between the ICRH and ICRH-SS for $\lambda_{max}^{pas} = [1 + r/(aA)]^{-1}$, with $A = 3$ is the aspect ratio of the torus, a the plasma radius.

Equation (22) is actually a restriction on the wave frequency: $\omega/(l\bar{\omega}_B) > (\lambda_{max}^{pas})^{-1}$. On the other hand, the upper border of the passing region is $\lambda_{max}^{pas} = \bar{B}/\max\{B(\mathbf{r})\}$, which follows from $|v_\parallel| = v\sqrt{1 - \lambda B(\mathbf{r})/\bar{B}}$. Here $\max\{B(\mathbf{r})\}$ is maximum of the magnetic field on the particle orbit. Taking this into account, we can write equation (22) as follows:

$$\frac{\omega}{l\bar{\omega}_B} > (\lambda_{max}^{pas})^{-1} = \frac{\max\{B(\mathbf{r})\}}{\bar{B}}. \tag{23}$$

Because $\bar{\omega}_B = \omega_B(\mathbf{r})\bar{B}/B(\mathbf{r})$, equation (23) reads:

$$\omega > \max\{l\omega_B(\mathbf{r})\}. \tag{24}$$

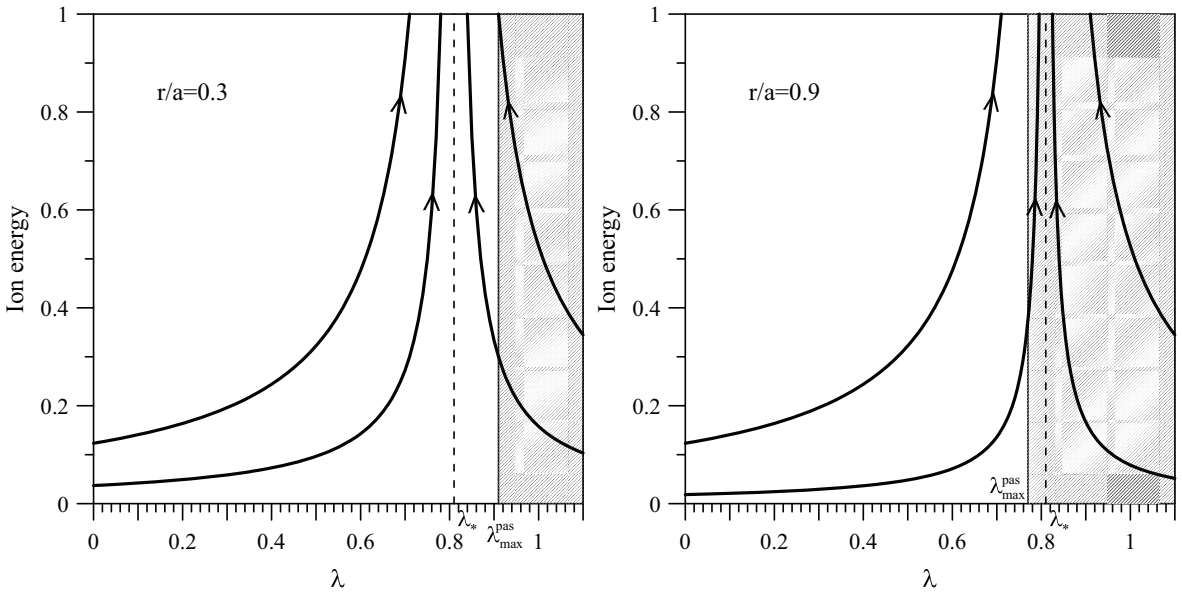

Figure 1. Quasilinear routes in the $(\lambda, \mathcal{E})$ space for $l = 1$ in JET. Here the region of trapped particles is shadowed, the separatrix is shown by dashed vertical line, the arrows show directions of the evolution during RF heating, the ion energy is measured in arbitrary units. The magnitude of $\lambda_* = 0.81$ (dotted line) is chosen in a way that $\lambda^{pas}_{max} > \lambda_*$ in the plasma core, $r/a < 0.7$ (the ICRH-SS case, left panel), whereas $\lambda^{pas}_{max} < \lambda_*$ at the periphery, $r/a > 0.7$ (the ICRH case, right panel). In the left panel, $\lambda^{pas}_{max} = 0.91$, which corresponds to $r/a = 0.3$; in the right panel $\lambda^{pas}_{max} = 0.77$, which corresponds to $r/a = 0.9$. We observe in the left panel that characteristics of passing particles do not intersect the trapped-passing border (λ^{pas}_{max}), in contrast to characteristics of trapped particles; in the right panel, characteristics of passing particles intersect the trapped-passing border.

This means that the particle orbits do not intersect the cyclotron resonance surface defined by $\omega = \omega_B(\mathbf{r})$ during ICRH-SS, in contrast to the cyclotron interaction during ICRH.

All the particles in a certain region satisfy equations (23), (24) when $\max\{B(\mathbf{r}\}$ is replaced by the maximum B in this region, B_{max}, so that

$$\tilde{\omega} > \frac{lB_{max}}{\bar{B}}, \tag{25}$$

with $\tilde{\omega} \equiv \lambda_*^{-1} = \omega/\bar{\omega}_B$.

On the other hand, ω should be not very high to avoid the influence of the $(l+1)$ harmonic and other cyclotron harmonics. This requirement is consistent with equations (23)-(25) for small l only. The magnitude $\lambda_* = 0.81$ used in figure 1 satisfies this condition, giving $\tilde{\omega} = 1.23$. This magnitude provides fulfillment of equation (25) in the plasma core, at least in the near-axis region, but may be not sufficiently high for plasma periphery where $B_{max}/\bar{B}$ is not very small, as was the case in figure 1.

Equation (24) implies that in the case of ICRH-SS the particles interact with the waves well away from the resonance surface determined by $\omega = l\omega_B(\mathbf{r})$. In tokamaks the magnetic field is maximum at the inner circumference of the torus. Therefore, in

order to heat the plasma core region, the cyclotron resonance $\omega = l\omega_B(\mathbf{r})$ should be well off-axis, close to high-field side of a flux surface located at the periphery or even outside the plasma.

The resonance condition (3) with the drift term neglected can be written as

$$\tilde{\omega} - lb(\mathbf{r}) = k_\parallel \rho_\parallel, \tag{26}$$

where $b(\mathbf{r}) = B(\mathbf{r})/\bar{B}$, $\rho_\parallel = v_\parallel/\bar{\omega}_B$. When $B = \bar{B}(1 - \epsilon\cos\vartheta)$ and $b_{max} \equiv \max\{B(\mathbf{r})\}/\bar{B} = 1 + \epsilon$, with $\epsilon = r/R$, the resonance (26) takes the form:

$$\Delta + l\epsilon(1 + \cos\vartheta) = k_\parallel \rho_\parallel, \tag{27}$$

where $\Delta = \tilde{\omega} - lb_{max}$ is a frequency excess required by equation (23). It follows from here that

$$\Delta \le k_\parallel \rho_\parallel \le \Delta + 2l\epsilon. \tag{28}$$

This equation shows that the required values of $k_\parallel \rho_\parallel$ are positive and lie in a certain range due to possible location of resonances at various poloidal angles. The minimum value of $k_\parallel \rho$ is Δ. It takes place when the resonance occurs at the high-field side of the torus ($\vartheta = \pi$).

When $b_{max}(r)$ is a growing function [the case for passing orbits in the field $B = \bar{B}(1 - \epsilon\cos\vartheta)$], the separatrix λ_l may coincide with λ^{pas}_{max} at a certain radius r_{border} representing a border between the ICRH and ICRH-SS. For instance, $r_{border} = 0.7a$ in figure 1. In the vicinity of r_{border}, $\Delta = 0$ and therefore the passing ions with small ρ can be accelerated without orbit transformation, but only those ions whose orbits lie at $r < r_{border}$.

Equations (27) - (28) give estimates for the required $k_\parallel \rho_\parallel$. To know exact magnitudes one has to take into account the particle drift velocity, especially for ions with high energy in the near-axis region.

Note that $\mathcal{E}_\parallel$ can considerably increase during ICRH-SS. To find the change of it we consider a particle at the moments when it passes points with a certain poloidal angle (e.g., $\vartheta = \pi/2$), in which case $\mathcal{E}_\parallel$ is a COM. Then the characteristic equation (21) can be written as $(\mathcal{E}\lambda_l - \mathcal{E} + \mathcal{E}_\parallel)_{\vartheta=\pi/2} = C_\mathcal{E}$, from which we obtain

$$\frac{\Delta\mathcal{E}_\parallel(\pi/2)}{\Delta\mathcal{E}} = 1 - \lambda_l. \tag{29}$$

For instance, for $\lambda_l = 0.8$ we have $\Delta\mathcal{E}_\parallel/\Delta\mathcal{E} = 1/5$.

Because only resonance ions are accelerated, the change of $\mathcal{E}_\parallel$ and, thus, the change of $\mathcal{E}$, depend on the spectrum of $k_\parallel$ of excited waves. Due to this, the range of energies of accelerated ions can be controlled by antenna power spectrum.

3.2. 3-D effects in ICRH-SS

Change of energy of a charged particle in an axisymmetric magnetic field leads to a change of its canonical angular momentum. Therefore, routes of quasilinear evolution

are three-dimensional. To describe them we supplement $\hat{\Pi}$ given by equation (2) with the terms associated with P_φ:

$$\hat{\Pi}^{(3D)} = \hat{\Pi} - \frac{n\mathcal{E}}{\omega}\frac{\partial}{\partial P_\varphi}. \tag{30}$$

This leads to additional characteristic equation:

$$nd\mathcal{E} = -\omega dP_\phi \tag{31}$$

and

$$n\mathcal{E} + \omega P_\phi = \text{const}. \tag{32}$$

The change of the canonical angular momentum implies that particles can move in radial direction during QL evolution.

Let us consider first the radial displacement of trapped particles. The longitudinal velocity of these particles vanishes at some points on the orbits. We will refer to these points as banana tips, although these points exist for both "banana" particles and "potato" particles (in the latter case, points where $v_\parallel = 0$ do not coincide with the turning points where $\dot{\vartheta} = 0$). It is clear that for these points

$$dP_\varphi = -\frac{e}{c}d\hat{\psi}_p, \tag{33}$$

where $\hat{\psi}_p = \psi_p(v_\parallel = 0)$ is a COM. Due to (33), it directly follows from equation (31) that a change of particle energy ($\Delta\mathcal{E}$) leads to a radial displacement of banana tips:

$$\Delta\hat{\psi}_p = \frac{cn}{e\omega}\Delta\mathcal{E}. \tag{34}$$

This is so-called "pinch effect" [12,13]. Bananas move inwards when $n < 0$ and outwards for $n > 0$. In order to evaluate this effect we use Boozer coordinates and define the radial coordinate r by $d\psi_T = \bar{B}rdr$, where ψ_T is the toroidal magnetic flux. Then $d\hat{\psi}_p = 0.5\bar{B}q^{-1}a^2d\psi$, where $\psi = r^2/a^2$, a is the plasma radius defined by $\psi = 1$, $q = q(\psi)$ is the tokamak safety factor. Displacement $\Delta\psi$ in this case can be written as

$$\Delta\psi = \sigma_n C_\psi \frac{\Delta\mathcal{E}}{\mathcal{E}_0}, \tag{35}$$

where $\sigma_n \equiv n/|n|$, $C_\psi = \langle q\rangle|n|\lambda_*\rho_0^2/a^2 > 0$, $\langle q\rangle$ is the average safety factor defined by $\int_{\psi_0}^{\psi} d\psi'/q(\psi') = \Delta\psi/\langle q\rangle$, $\Delta\psi = \psi - \psi_0$, $\rho = v/\bar{\omega}_B$, the subscript "0" labels the initial particle energy / velocity. It follows from here that the particle displacement is proportional to a small value, ρ_0^2/a^2, but it can be considerable due to $n \gg 1$ when $\Delta\mathcal{E} > \mathcal{E}_0$.

Dependence of ψ on λ can be obtained from equation (35) by means of equation (20), which leads to

$$\frac{\Delta\mathcal{E}}{\mathcal{E}_0} = \frac{\lambda_0 - \lambda}{\lambda - \lambda_l}. \tag{36}$$

We obtain:

$$\Delta\psi = \sigma_n C_\psi \frac{\lambda_0 - \lambda}{\lambda - \lambda_l} \tag{37}$$

and

$$\frac{d\psi}{d\lambda} = -\sigma_n C_\psi \frac{\lambda_0 - \lambda_l}{(\lambda - \lambda_l)^2}. \tag{38}$$

Note that $\lambda_0 - \lambda_l > 0$ and $\lambda \neq \lambda_l$ *for all trapped particles* during ICRH-SS. Therefore, $\psi(\lambda)$ is a growing / decreasing function for $n < 0$ / $n > 0$.

Now we proceed to passing particles. We consider the influence of RF field on the radial motion of a point on the particle orbit at a certain poloidal angle, ϑ_1, which particle crosses after successive transits. Then

$$dP_\varphi = RMdv_\parallel + Mv_\parallel dR_r - \frac{e}{c}d\psi_p, \tag{39}$$

where all the magnitudes are taken at ϑ_1, and $dR_r = (\partial R/\partial r)dr$. We have to express $dv_\parallel$ through $d\mathcal{E}$ and dr. With this purpose we use the relation $\mathcal{E}_\parallel = \mathcal{E}(1 - \lambda b)$, with $b = B(\mathbf{r})/\bar{B}$, from which we can write

$$d\mathcal{E}_\parallel = (1 - b\lambda)d\mathcal{E} - \mathcal{E}bd\lambda - \mathcal{E}\lambda db_r, \tag{40}$$

where $db_r = (\partial b/\partial r)dr$. Eliminating $d\lambda$ here by means of characteristic equation (20) we have

$$Mv_\parallel dv_\parallel = (1 - b\lambda_l)d\mathcal{E} - \mathcal{E}\lambda db_r. \tag{41}$$

Combining this equation with equation (39) and using characteristic equation $dP_\varphi = -(n/\omega)d\mathcal{E}$ we obtain the following:

$$Rd\mathcal{E}\left(1 - b\lambda_l + \frac{nv_\parallel}{\omega R}\right) = dr\left[\frac{ev_\parallel}{c}\frac{d\psi_p}{dr} - (2\mathcal{E}_\parallel + \mathcal{E}\lambda)\cos\vartheta_1\right]. \tag{42}$$

One can see that the first term in the RHS of this equation dominates when

$$r \gg q\rho_\parallel. \tag{43}$$

We assume that this is the case and take into account that only resonant particles undergo QL evolution. Then, writing the resonance (26) as

$$1 - b\lambda_l = \frac{k_\parallel v_\parallel}{\omega} \tag{44}$$

and using $k_\parallel = (m - nq)/qR$ (m is the poloidal mode number, q is the tokamak safety factor), we reduce equation (42) to

$$d\psi_p = \frac{cm}{e\omega q}d\mathcal{E}. \tag{45}$$

This equation has the form similar to that of equation (34) for trapped particles. It formally can be obtained from (34) by replacing n with m/q.

It is of importance, that $d\psi_p/d\mathcal{E}$ of passing particles is determined by the poloidal, rather than toroidal, wave number, in contrast to that of trapped particles.

The particle velocity $v_\parallel$ changes during QL evolution. For this reason, the particle radial displacement $\Delta\psi_p$ which can be obtained from equation (45) is correct only for small change of $v_\parallel$. In general, equation (42) [rather than (45)] should be integrated with subsequent use of the resonance condition for finding $\Delta\psi_p$.

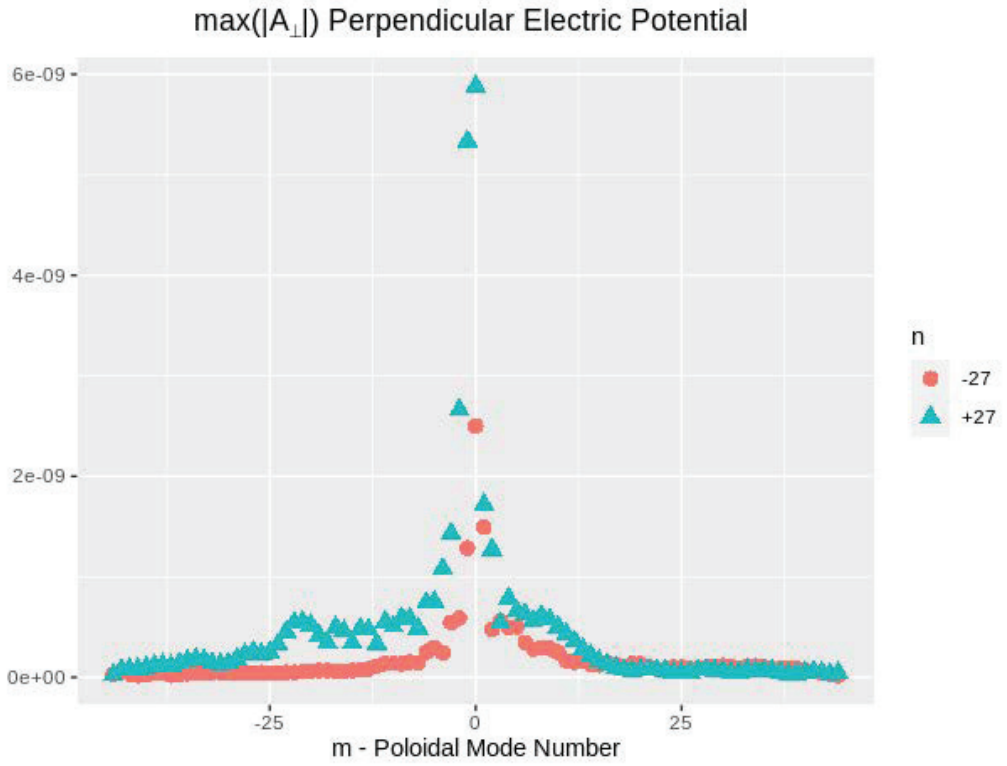

Figure 2. Max $|\mathbf{A}_\perp|$ versus poloidal wavenumbers in JET discharge # 91256 for $n = \pm 27$, which was calculated by SCENIC. Notation: Max $|\mathbf{A}_\perp|$ is the maximum value of $A_\perp$ over the radial grid, $\mathbf{A}_\perp$ is transverse vector potential of the electromagnetic field.

Let us consider a numerical example. We take $l = 1$, $\bar{B} = 3$ T, $R = 3$ m, $\Delta\mathcal{E}/\mathcal{E}_0 = 10$, $\mathcal{E}_0 = 100$ keV, $a = 1$ m, $\tilde{\omega} = 1.23$, $\langle q \rangle = 1.5$. Using equation (35) with $n = 27$ (which corresponds to a maximum of the power spectrum in the JET antenna with dipole phasing) we obtain $|\Delta\psi| = 0.1\langle q \rangle$ for trapped particles.

The displacement of passing particles depends on the poloidal wave numbers which are typically small and both positive and negative m may be present. In particular, the SCENIC modelling of the JET discharge #91256 shows that $m = 0$ mainly contributes, see figure 2 where the wave numbers of the RF field are presented. This implies that displacement of injected passing ions is negligible in this discharge. In contrast to wave numbers, the wave amplitude, δE, does not affect the ways of the ion acceleration. However, it plays an important role in power absorption. The SCENIC code predicts δE that lies in the range $(1 - 4)$ kV/m in the region of interest, $0.1 \lesssim r/a \lesssim 0.6$, see figure 3.

A 3-D picture of QL evolution for $m = 0$, which is based on the analysis above, is shown in figure 4.

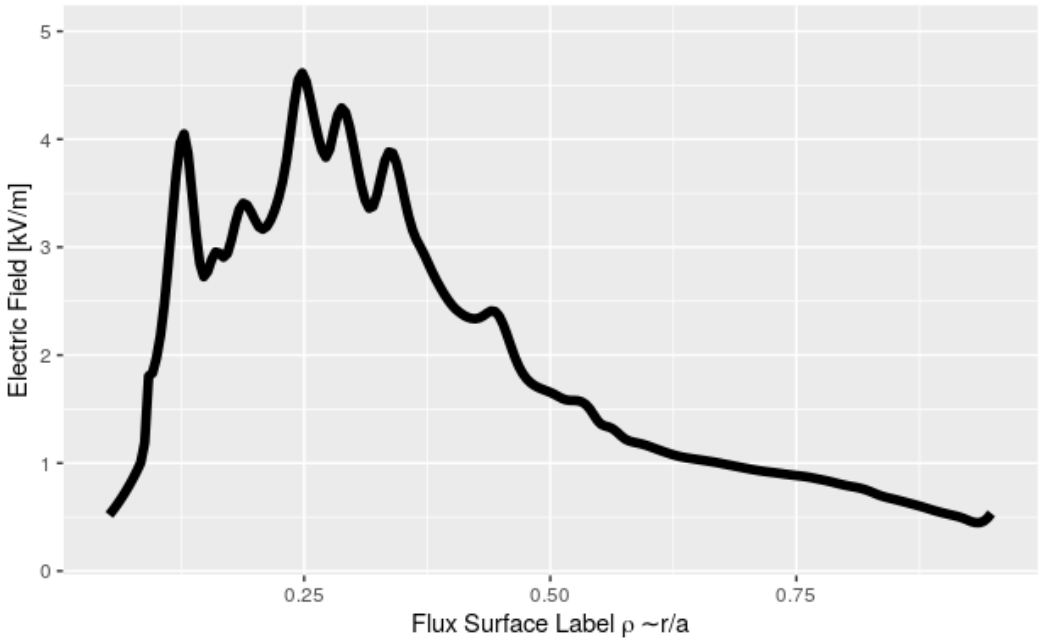

Figure 3. The RF wave amplitude versus radius in JET discharge # 91256 calculated by SCENIC.

4. Conditions mitigating effects of collisions

4.1. Quasilinear and collisional fluxes

In this section we consider behavior of passing ions during ICRH-SS with taking into account Coulomb collisions. As shown above, these ions remain passing when they are located in the region $r < r_{border}$ and move along QL characteristics. However, collisional pitch-angle scattering may lead to orbit transformation, making these particles trapped. Therefore, it is of importance to find conditions which should be satisfied to minimize this detrimental effect of collisions.

We consider passing particles and restrict ourselves to 2-D approximation, assuming that their radial displacement is small. Particles with the energies $\mathcal{E} > \mathcal{E}_c$ will be considered. Here $\mathcal{E}_c \sim (M_i/M_e)^{1/3}T_e$ (subscripts e and i label electrons and ions, respectively, M is the particle mass, T is the temperature) is the energy above which the collision slowing down dominates the scattering.

A quasilinear equation for distribution function of fast ions is

$$\frac{\partial F}{\partial t} = Q(F) + C(F) + S, \tag{46}$$

where $Q(F)$ and $C(F)$ are the quasilinear term and collisional term, respectively, and S is a source function.

Passing particles avoid transformation into trapped ones during ICRH-SS when the λ component of quasilinear flux in the plane $(\lambda, \mathcal{E})$ exceeds the corresponding collisional flux. Due to the fact that the separatrix λ_l is located in the region of passing particles

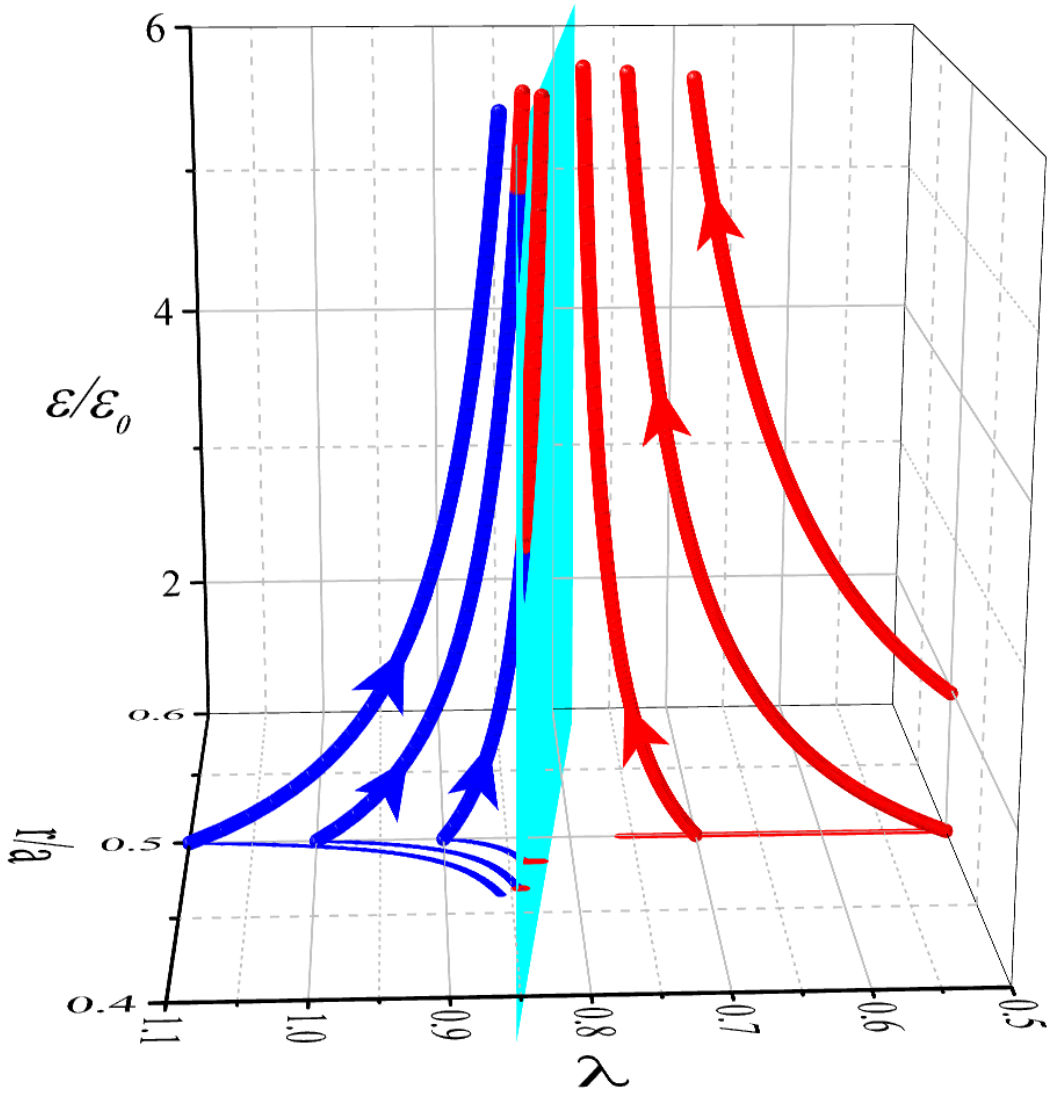

Figure 4. 3-D routes of QL acceleration of particles with $r_0/a = 0.5$, $\mathcal{E}_0 = 100$ keV, and various λ_0: 0.2, 0.5, 0.7 (passing particles) and 0.9, 1.0, 1.1 (trapped particles) in JET with the same parameters as in figure 1 and $n = -27$, $m = 0$ during ICRH-SS. We observe that routes of trapped particles (thick blue curves) intersect the cyan plane representing trapped-passing border (except for deeply trapped particles, $\lambda_0 = 1.1$) and then follow passing routes. Passing particles do not move radially, whereas trapped particles move inwards but their displacement is rather small; this is clearly seen due to shown projections of the routes to the plane (r, λ) (red and blue thin lines for passing and trapped particles, respectively).

in the case of ICRH-SS, one does not need to consider the region of trapped particles. Therefore, we can use the quasilinear operator (10) describing QL evolution of passing particles.

The sum $Q(F) + C(F)$ can be written as follows:

$$Q(F) + C(F) = -\frac{1}{\sqrt{g}} \left(\frac{\partial}{\partial \mathcal{E}} \sqrt{g} J_{\mathcal{E}} + \frac{\partial}{\partial \lambda} \sqrt{g} J_{\lambda} \right), \tag{47}$$

where $J_{\mathcal{E}}$ and J_{λ} are components of the particle flux, $\mathbf{J}$, produced by both the wave-particle interaction and Coulomb collisions, $\mathbf{J} = \mathbf{J}^Q + \mathbf{J}^C$, where the superscripts Q and C label the flux quasilinear part and collisional part, respectively.

Components of the quasilinear flux are

$$J^Q_{\mathcal{E}} \equiv \mathcal{E} J \tag{48}$$

and

$$J^Q_{\lambda} \equiv (\lambda_l - \lambda) J, \tag{49}$$

with

$$J = -D_{\mathcal{E}} \hat{\Pi} F = -\mathcal{K} \lambda \mathcal{I}_l^2 \left(\frac{\partial F}{\partial \mathcal{E}} + \frac{\lambda_l - \lambda}{\mathcal{E}} \frac{\partial F}{\partial \lambda} \right), \qquad D_{\mathcal{E}} = \mathcal{K} \frac{\lambda \mathcal{I}_l^2}{\mathcal{E}}. \tag{50}$$

It follows from equations (48), (50) that $J^Q_{\mathcal{E}} > 0$ when the magnitude in brackets of equation (50) is negative. For RF-energy absorption to take place independently on the sign of $(\lambda_l - \lambda)$, the first term in the brackets should dominate, with $\partial F / \partial \mathcal{E} < 0$. This implies that particles are accelerated, absorbing the wave energy, in this case. On the other hand, the sign of the first term in the relation for the λ flux depends on the sign of $(\lambda_l - \lambda)$, whereas the sign of the second one does not:

$$J^Q_{\lambda} = -\sum_k \mathcal{K} \lambda \mathcal{I}_l^2 \left[(\lambda_l - \lambda) \frac{\partial F}{\partial \mathcal{E}} + \frac{1}{\mathcal{E}} (\lambda_l - \lambda)^2 \frac{\partial F}{\partial \lambda} \right]. \tag{51}$$

Because the first term dominates during power absorption, the flux J^Q_{λ} is positive when λ is small, $\lambda < \lambda_l$, and negative when $\lambda > \lambda_l$. Therefore, it tends to approach particles to the separatrix $\lambda = \lambda_l$, independently on their location with respect to the separatrix. This conclusion agrees with the picture shown in figure 1.

The collision operator for particles with $\mathcal{E} > \mathcal{E}_c$ can be written in the form [11]:

$$C(F) = \frac{1}{\tau_{\mathcal{E}} \sqrt{\mathcal{E}}} \frac{\partial}{\partial \mathcal{E}} \left(\mathcal{E}^{3/2} + \mathcal{E}_c^{3/2} \right) F + \frac{2\alpha}{\tau_{\mathcal{E}}} \frac{\mathcal{E}_c^{3/2}}{\mathcal{E}^{3/2}} \sqrt{1-\lambda} \frac{\partial}{\partial \lambda} \lambda \sqrt{1-\lambda} \frac{\partial}{\partial \lambda} F, \tag{52}$$

where

$$\alpha = \frac{n_e Z_{ef}}{2M \sum_i n_i Z_i^2 / M_i},$$

$\tau_{\mathcal{E}} = (\nu_{\mathcal{E}})^{-1}$ is the collisional energy loss time, Z is the electric charge number, Z_{ef} is the effective charge number, M is the fast ion mass. This equation determines the flux with components

$$J^C_{\mathcal{E}} = -\frac{1}{\tau_{\mathcal{E}}} \frac{\mathcal{E}^{3/2} + \mathcal{E}_c^{3/2}}{\sqrt{\mathcal{E}}} F, \quad J^C_{\lambda} = -\frac{2\alpha}{\tau_{\mathcal{E}}} \frac{\mathcal{E}_c^{3/2}}{\mathcal{E}^{3/2}} \lambda (1-\lambda) \frac{\partial F}{\partial \lambda}. \tag{53}$$

4.2. Absorbed power and average $\mathcal{K}$

Let us derive a relation for the absorbed RF power as a function of the wave electric field. It will be used later to evaluate the quasilinear flux J_λ^Q.

The simplest way to do it is to introduce new variables by replacing the pitch λ with the characteristic $\xi = \mathcal{E}(\lambda_l - \lambda)$. Then equation (2) reduces to $\hat{\Pi} = \mathcal{E}\partial/(\partial\mathcal{E})$ and QL operator takes the form:

$$Q = \frac{1}{\sqrt{g_\xi}}\frac{\partial}{\partial\mathcal{E}}\sqrt{g_\xi}\,\mathcal{K}\mathcal{E}\lambda\mathcal{I}_l^2\frac{\partial F(\mathcal{E},\xi)}{\partial\mathcal{E}}, \tag{54}$$

where $\sqrt{g_\xi} = 2\pi/(M^2|v_\parallel|)$, with $v_\parallel = v_\parallel(\mathcal{E},\xi)$. In these variables the absorbed power density, $P_{rf} = \int d^3v\mathcal{E}Q(F)$, can be written as

$$P_{rf} = \int_0^\infty d\mathcal{E}\int d\xi\mathcal{E}\frac{\partial}{\partial\mathcal{E}}\sqrt{g_\xi}\,\mathcal{K}\mathcal{E}\lambda\mathcal{I}_l^2\frac{\partial F(\mathcal{E},\xi)}{\partial\mathcal{E}}. \tag{55}$$

Integrating over $\mathcal{E}$ by parts twice we obtain:

$$P_{rf} = \int d^3vF\frac{1}{\sqrt{g_\xi}}\frac{\partial}{\partial\mathcal{E}}\left(\sqrt{g_\xi}\,\mathcal{K}\mathcal{E}\lambda\mathcal{I}_l^2\right). \tag{56}$$

Only resonant ions contribute to P_{rf}. Therefore, we replace integral $\int d^3v(...)$ over the whole velocity space of passing ions with the integral over resonance region, $\int_{res} d^3v(...)$. Then we introduce an average magnitude $\bar{\mathcal{K}}$ for these particles, writing equation (56) as follows:

$$P_{rf} = \bar{\mathcal{K}}\int_{res} d^3vF\frac{1}{\sqrt{g_\xi}}\frac{\partial}{\partial\mathcal{E}}\left(\sqrt{g_\xi}\,\mathcal{E}\lambda\mathcal{I}_l^2\right) \tag{57}$$

or

$$P_{rf} = \bar{\mathcal{K}}n_{res}\lambda_{ave}, \tag{58}$$

where

$$\lambda_{ave} = \left\langle\frac{1}{\sqrt{g_\xi}}\frac{\partial}{\partial\mathcal{E}}\left(\sqrt{g_\xi}\,\mathcal{E}\lambda\mathcal{I}_l^2\right)\right\rangle \tag{59}$$

$\lambda = \lambda_l - \xi/\mathcal{E}$, $\mathcal{I}_l$ contains Bessel functions $J_{l\pm1} = J_{l\pm1}(z)$, $z = k_\perp v_\perp/\bar{\omega}_B$, $v_\perp = \sqrt{2(\mathcal{E}\lambda_l - \xi)/M}$, brackets denote averaging with the distribution function F/n_{res}, n_{res} is the number of resonant particles defined by $n_{res} = \int_{res} d^3vF$.

One can see that $\partial z/\partial\mathcal{E} = \lambda_l z/(2\mathcal{E}\lambda)$ and

$$\frac{1}{\sqrt{g_\xi}}\frac{\partial}{\partial\mathcal{E}}(\sqrt{g_\xi}\mathcal{E}\lambda) = 0.5\lambda_l\left(1 + \frac{1-\lambda/\lambda_l}{1-\lambda}\right). \tag{60}$$

Taking this into account we obtain for the case when the E_+ term in the diffusion coefficient dominates (i.e., $\eta_l = 1$):

$$\lambda_{ave} = \left\langle 0.5J_{l-1}\left[J_{l-1}\left(\lambda_l + \frac{\lambda_l - \lambda}{1-\lambda}\right) + 2\lambda_l z J'_{l-1}\right]\right\rangle. \tag{61}$$

For $l = 1$ and $z < 1$ it is reduced to

$$\lambda_{ave} = \left\langle 0.5\lambda_l\left(1 + \frac{1-\lambda/\lambda_l}{1-\lambda}\right)\right\rangle. \tag{62}$$

Equations (58), (61), and (62) are obtained in the $\mathcal{E},\xi$ variables [with $\lambda = \lambda(\mathcal{E},\xi)$]. However, they are valid also in the $\mathcal{E},\lambda$ variables because they are written in the form that does not contain the metric tensor determinant explicitly.

4.3. Ratio of fluxes

To proceed, we have to specify the source term in equation (46). We assume that fast ions are produced by neutral beam injection (NBI), and they are peaked around $\lambda = \lambda_\alpha$, with $\lambda_\alpha < \lambda_l$. In this case, the collisional pitch-angle scattering will spread the particle distribution, leading to $F \neq 0$, with $\partial F/\partial\lambda < 0$ at $\lambda > \lambda_\alpha$. Therefore, in the region $\lambda > \lambda_l$ the collisional flux J^C_λ will compete with the quasilinear flux, see figure 5. We request $|J^Q_\lambda| > J^C_\lambda$ in this region to avoid production of trapped particles by collisions.

We keep only the first term in equation (51) for J^Q_λ, which should dominate to provide heating in the region $\lambda > \lambda_l$. Then we obtain the following ratio of $|J^Q_\lambda/J^C_\lambda|$ determined by equations (51), (53):

$$\frac{J^Q_\lambda}{J^C_\lambda} = \frac{\mathcal{K}(\lambda_l-\lambda)\mathcal{I}_l^2\tau_\mathcal{E}\mathcal{E}^{3/2}\partial F/\partial\mathcal{E}}{2\alpha(1-\lambda)\mathcal{E}_c^{3/2}\partial F/\partial\lambda}. \tag{63}$$

This equation with $\mathcal{K}$ given by (17) reads:

$$\left|\frac{J^Q_\lambda}{J^C_\lambda}\right| = \frac{2\bar\omega_B\tau_\mathcal{E}}{\alpha}\frac{R}{\rho_c}\frac{|\lambda_l-\lambda|\lambda_{ef}}{(1-\lambda)^{3/2}}\frac{\mathcal{E}}{T_{ef}}\frac{v_E^2}{v_c^2}\mathcal{I}_l^2\Delta\vartheta, \tag{64}$$

where $v_E = cE_+/\bar B$ is the drift velocity in the wave field and equilibrium magnetic field, $v_c = \sqrt{2\mathcal{E}_c/M}$; $\rho_c = v_c/\bar\omega_B$, T_{ef}, λ_{ef}, and $\Delta\vartheta$ are defined by $T_{ef}^{-1} = |d\ln F/d\mathcal{E}|$, $|\lambda_{ef}^{-1}| = -d\ln F/d\lambda$, and $\Sigma_j\int d\vartheta_j|E_j|^2 = E_+^2\Delta\vartheta$, respectively.

It is possible to present the ratio of fluxes in a form more suitable for estimates.

This can be done by using the average value $\bar{\mathcal{K}}$ instead of $\mathcal{K}$, and taking into account that P_{rf} is associated with the density of resonant ions and their maximum energy, $\mathcal{E}_m$, as follows:

$$P_{rf}\tau_\mathcal{E} = n_{res}\mathcal{E}_m. \tag{65}$$

Due to this equation and (58), $\bar{\mathcal{K}}$ reduces to $\bar{\mathcal{K}} = \mathcal{E}_m/(\tau_\mathcal{E}\lambda_{ave})$. Then equation (63) reads:

$$\left|\frac{J^Q_\lambda}{J^C_\lambda}\right| = \frac{\mathcal{E}_m}{2\alpha T_{ef}}\frac{|\lambda_l-\lambda|\lambda_{ef}}{(1-\lambda)\lambda_{ave}}\mathcal{I}_l^2\frac{\mathcal{E}_m^{3/2}}{\mathcal{E}_c^{3/2}}. \tag{66}$$

Let us evaluate the obtained flux ratio for $\lambda_l < \hat\lambda < \lambda^{pas}_{max}$. We take $l = 1$ and $J_{l-1} = 1$, $\eta_l = 1$, $\lambda = \lambda^{pas}_{max} = 0.9$, $\lambda_l = 0.8$, $\hat\lambda = 0.85$, $\lambda_\alpha = 0.6$. The accelerated ions lie in the range $\lambda > \lambda_\alpha$. Therefore, $(\lambda^{pas}_{max} - \lambda_\alpha) \lesssim \lambda_{ef} < \infty$, depending on QL distortion of $F(\lambda)$. It is clear that when λ_{ef} is very large (i.e., when λ-plateau is formed), the effect of collisions is negligible. In contrast, we consider an unfavorable case, taking $\lambda_{ef} = 0.3$. To evaluate λ_{ave} we take into account that the integrand in (59) is a monotonically decreasing function of λ, it equals 0.65, 0.4, 0.23 at $\lambda = \lambda_\alpha$, λ_l, $\hat\lambda$, respectively, and less

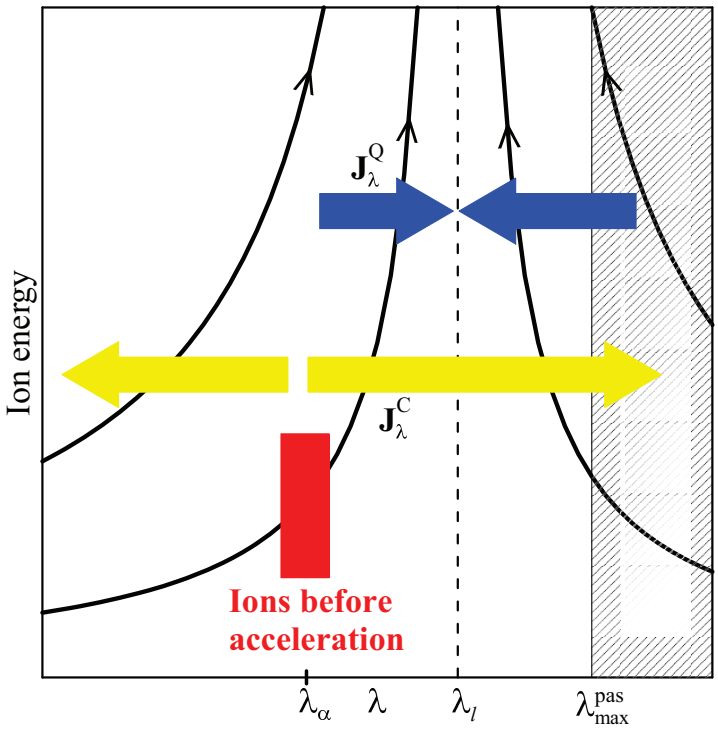

Figure 5. Sketch of quasilinear and collisional fluxes along λ during ICRH-SS applied to NBI ions with the pitch parameters close to λ_α. Red rectangle show the region where fast ions are born due to NBI, arrows show directions of λ components of the QL flux (blue) and collisional flux (yellow). We observe these fluxes have different directions in the region $\lambda > \lambda_l$.

than 0.2 for $\lambda > \hat{\lambda}$. Therefore, it is reasonable to take $\lambda_{ave} = 0.4$. Then $\lambda_{ave}/\lambda_{ef} = 1.3$. In addition, we take $\mathcal{E}_m/(2\alpha T_{ef}) = 1$. For these parameters, $J_\lambda^Q \gg J_\lambda^C$ provided that $\mathcal{E}_m/\mathcal{E}_c \gg 2$.

5. SCENIC modelling

In order to demonstrate practical feasibility of ICRH-SS and its difference from conventional ICRH, the JET discharge #91256 was selected, which was studied in details in references [3, 4, 14]. This JET pulse used hydrogen as the main gas, and also was an L-mode discharge. Although it was designed as a demonstration of the 3-ion species scheme [15], it also complies with the criteria of the ICRH-SS scheme. In this section, simulations of this discharge will explore a comparison between the ICRH-SS JET discharge #91256 and the same discharge but with an artificial decrease of the RF-antenna frequency.

Numerical simulation was carried out using the SCENIC package [5]. In SCENIC, the Monte-Carlo simulations solve the Fokker Planck equation by using an accurate 3D representation of the actual JET NBI injector and the ICRF antenna geometries. The NBI ionization profile is calculated based upon the background plasma profiles and plasma shape, which then generates the Monte-Carlo marker population. RF-wave

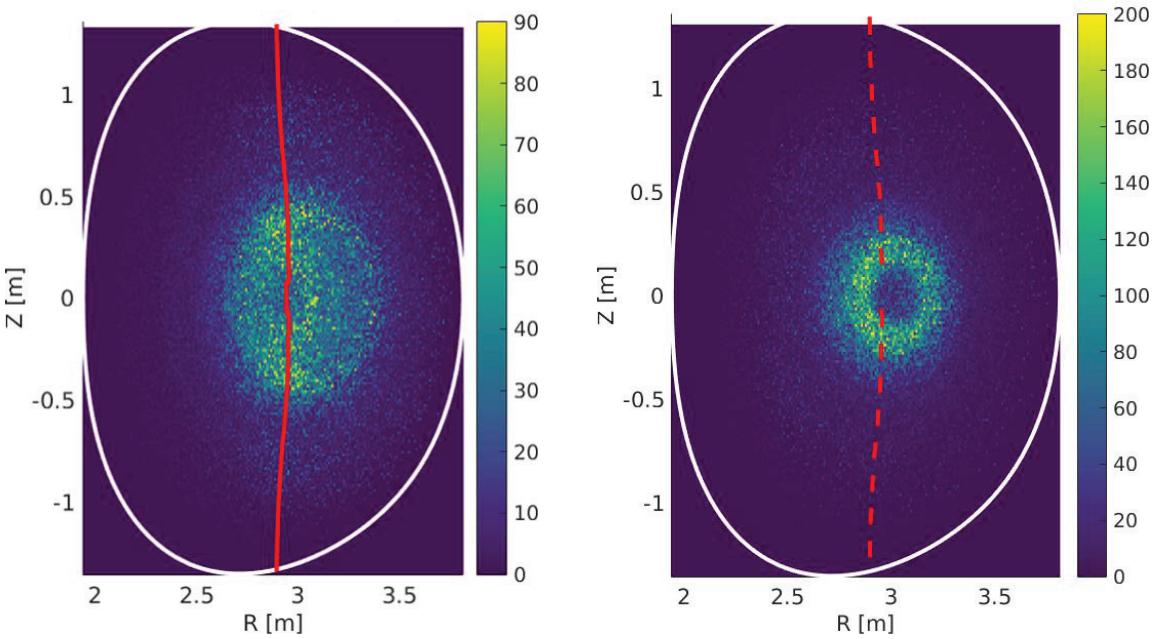

Figure 6. Fast ion pressures formed during ICRH (left panel) and ICRH-SS (right panel) in SCENIC simulations of a JET hydrogen-majority plasma. Fast ion pressure is normalized by volume $W_{fast}(R,Z)/(2\pi\int\sqrt{g}dRdZ)$. Calculations were carried out (right) for the antenna frequency 25 MHz which provided on-axis heating of 100 keV NBI ions due to Doppler-shifted $l=1$ resonance (satisfying the condition $\lambda_* < \lambda_{max}^{pas}$) shown by red dashed line, and (left) for the frequency artificially reduced by a factor of 1.19 to simulate fundamental conventional ICRH heating of minority ions (deuterons) with the resonance shown by red solid line.

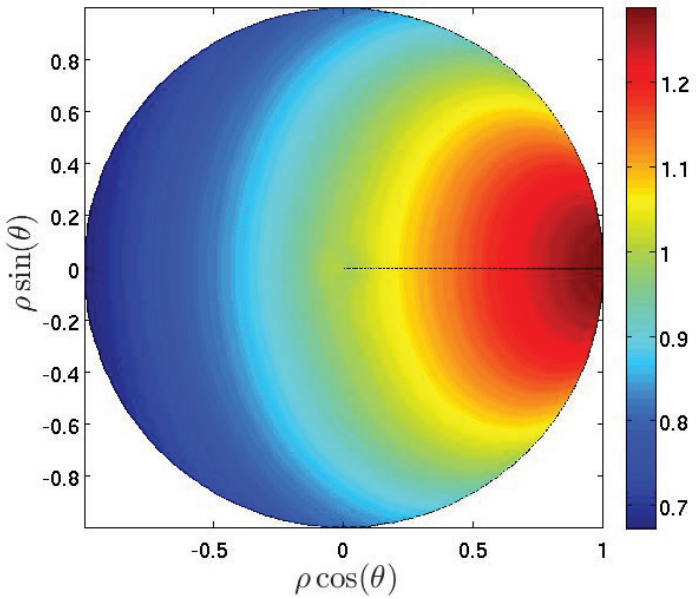

Figure 7. Contour plot of $b = B(\mathbf{r})/\bar{B}$ of the JET simulations. The flux coordinates applied allow a comparison with figure 6 of [2].

propagation and absorption is calculated using LEMan [16] through the plasma dielectric tensor and the hot plasma dispersion relation. For the simulations presented here, the wave-propagation LEMan code retained only first order Finite Larmor Radius (FLR) effects. Therefore, no mode-conversion or harmonic ($n > 1$) effects are included in the wave-propagation and absorption simulations made by LEMan. TORIC [17] simulations showed that electron RF-power absorption through mode conversion effects was a minority $\sim 10\%$ for the case of ICRH-SS in JET shot #91256 [18]. The RF-antenna and NBI geometry are localized in three-dimensional space, which is important to accurately calculate synergetic RF-wave heating of the NBI ions. ICRF-NBI synergetic heating is modelled via the quasilinear operator described in [19], which evaluates the interactions between the RF-wave and the Monte Carlo marker population when the resonance condition (equation (1)) is fulfilled. A more detailed explanation of the SCENIC modelling of ICRF-NBI synergetic heating schemes is given in section 5.2 in [20] with the title 'fast-splitting method'. Agreement between SCENIC simulations and JET experimental measurements for the total neutron rate and the energy distribution of the fast ions is shown in a recent work [4].

The results of our simulations for ICRH and ICRH-SS are presented in figures 6 - 9. Plasma profiles taken from the JET simulations of [3,4] were taken for these simulations. The profiles are described in section 5.2.3 of [20]. The core electron temperature and density were 4.2 keV and $4.1 \times 10^{19} m^{-3}$, respectively. Plasma current was 1.9 MA and on-axis magnetic field was 2.88 T. The core ion temperature was assumed to be 3.5 keV.

The deuterium density was taken as $\sim$ 15% of the total ion populations; 0.4% beryllium was included in the simulations as an assumed inherent impurity which is often found in JET experiments. The auxiliary heating power for NBI and ICRF used in the simulations is 3.2MW and 2.5MW respectively. The ICRF antenna frequency 25 MHz results in ICRH-SS in the plasma core; but simulations have also been made with $f = 21$ MHz with all other plasma parameters held constant to model conventional ICRF scheme that does not rely on the enlarged Doppler-shifted term for core heating. The core $k_{\|}$ values lie between 8-10 m^{-1} and 7-9 m^{-1} for the ICRH-SS and ICRH schemes respectively. The NBI injector geometry results in freshly ionized particles with $\chi_{NBI} \sim 0.51$, which gives $\lambda_{NBI} \sim 0.74$.

The JET magnetic geometry results in

$$\lambda_{max}^{pas} = 0.9 - 0.94 \text{ for } 0.2 \lesssim r/a \lesssim 0.3, \tag{67}$$

$\lambda_{max}^{pas} = 0.86$ for $r/a = 0.5$, and

$$\lambda_{max}^{pas} = 0.76 - 0.86 \text{ for } 0.5 \lesssim r/a \lesssim 1. \tag{68}$$

The choice of the antenna frequency for the two simulations gives $\lambda_* \approx 0.87$ in the case of ICRH-SS (25MHz) and $\lambda_* \approx 1$ for ICRH (21MHz). This implies that the ICRH-SS condition $\lambda_* < \lambda_{max}^{pas}$ is satisfied in discharge #91256, but only in the region $r/a < 0.5$. In this region the power density deposition is maximum and well exceeds that of the discharge with reduced frequency, as shown in figure 9; this core region plays the main role also because most accelerated ions are located here. That is why we can say that

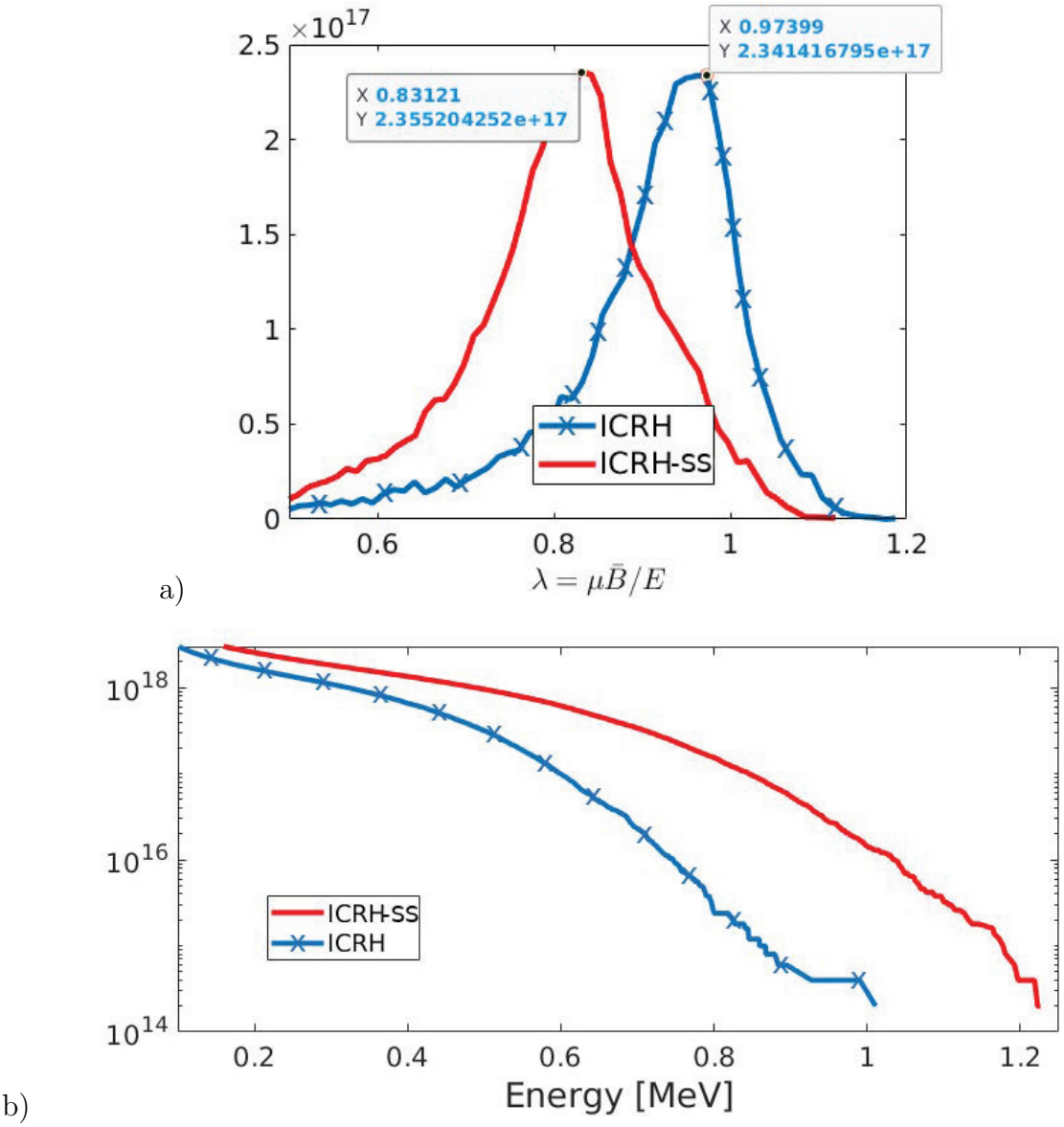

Figure 8. A comparison of the energetic particles produced in the JET simulations using the ICRH and ICRH-SS scheme in blue and red respectively. a) the number of particles [a.u.] against λ, with annotations for the peak values. b) the number of particles [a.u.] against energy[MeV]. Both plots restrict the ions used to have $\mathcal{E}$ >100keV and $s \equiv \psi_{tor}/\psi_{tor,edge} < 0.6$.

discharge # 91256 complies with the ICRH-SS criteria, although its periphery does not (as in figure 1, right panel).

Figure 7 illustrates the magnetic field strength contours in flux coordinates, which can be used in combination with equation (26) to interpret the RF-resonance condition: for ICRH heating, freshly injected NBI ions ($v_{\|} \sim 2 \times 10^6$ m s^{-1}) can only resonate with the RF-wave on the LFS. However, by increasing the RF-antenna frequency to 25MHz for ICRH-SS heating, NBI ions can resonate with the wave on-axis.

The particle orbits shown in figure 6 (right panel) pass rather close to the magnetic

axis. Nevertheless, the orbits of NBI ions before acceleration ($\mathcal{E} \leq 100$ keV) and after weak acceleration are standard. To see it we note that the near-axis 100 keV ions with $\chi = 0$ reach the flux surface radius $r_{max} = \hat{s}^{2/3}R = 14$ cm. Deflection from the magnetic axis of co-injected particles with $\chi \sim 0.6$ can be evaluated as $r_{max} \sim 10$ cm. This is less by a factor of 2 than maximum deviation of particles, ~ 20 cm, in figure 6. Moreover, one can directly see that the orbit width in figure 6 (right panel) is considerably less than orbit average radius. However, orbits after strong acceleration, e.g. when $\mathcal{E} \sim 1$ MeV, become non-standard. For these ions trapped-passing boundary is absent (they are co-passing), and λ_{max}^{pas} becomes meaningless. The number of these ions is small and therefore their orbits cannot be identified in the figure.

The SCENIC simulations reflect differences in the energetic particle ($\mathcal{E} > 100$keV) population produced by both the ICRH and ICRH-SS schemes, shown in figure 8. The energetic particle distribution function, shown in figure 8b indicates that the ICRH-SS scheme generates larger highly energetic ion populations than ICRH, with almost two orders of magnitude more particles at 1MeV. The λ values of the energetic particles in the core region are shown in figure 8 (upper panel), indicating that the quasilinear diffusion in parallel velocity space is evidently higher for the ICRH-SS scheme than for ICRH. The peak value $\lambda \sim 0.83$ for the ICRH-SS scheme satisfies the condition for Doppler-shifted resonance shown in equation (28). From the fast ion pressure plots in figure 6, the energetic particle trajectories visibly reflect the increase in quasilinear parallel velocity diffusion: energetic fast ions tend to be pushed more into trapped orbits for ICRH than for ICRH-SS. The ICRH scheme (left) shows banana orbits, whereas ICRH-SS (right) illustrates passing orbits that encircle the magnetic axis. Thus, in the considered examples, ICRH-SS reduces the trapped particle fraction and significantly increases the number of energetic passing particles; the fast ion pressure in the core is more than doubled due to ICRH-SS.

Note that the condition $|J_\lambda^Q / J_\lambda^C| \gg 1$ is easily satisfied [we used equation (66) and figure 8 (lower panel) from which the evaluated effective temperature $T_{ef} \sim 130 - 150$ keV in the ICRH-SS scheme and less in ICRH]. This means that collisions did not prevent the ion approach the separatrix during acceleration, which agrees with the presence of maxima close to separatrices in figure 8 (upper panel). These maxima lie not exactly at λ_* because the separatrices correspond to infinite energy.

The critical energy of deuterium ions is a parameter given by the background plasma profiles, which indicates that if the deuterium ion has an energy above this value then the collisional energy exchange is dominated by the electrons rather than the background hydrogen:

$$\mathcal{E}_{crit} = 14.8 A_{NBI} T_e \left[\sum_j \frac{n_j Z_j^2}{n_e A_j} \right]^{(2/3)}, \tag{69}$$

where j is each of the ion species present in the plasma, A is the atomic number and Z is the atomic charge. For these JET simulations, $\mathcal{E}_{crit} \sim 110$ keV in the plasma core. This implies that the use of ICRH-SS may increase the amount of power transferred to the

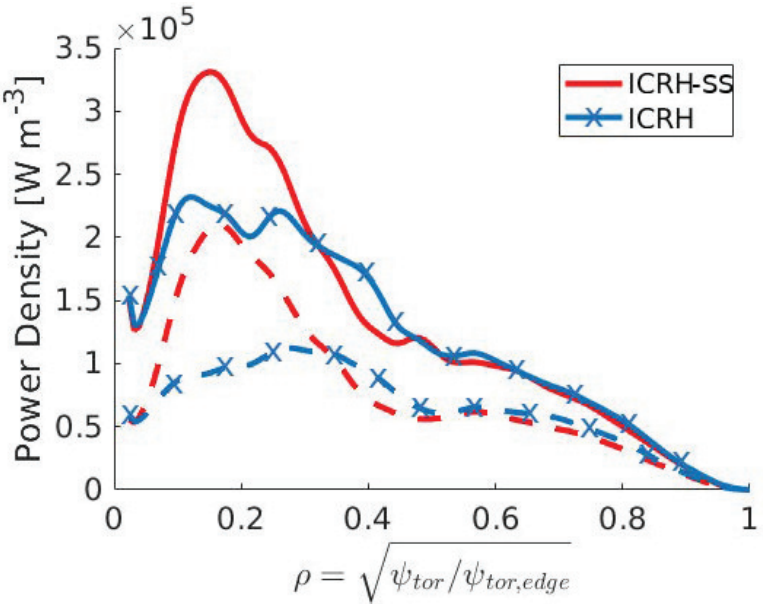

Figure 9. Collisional power density transferred from the NBI ions to the background plasma, comparing the ICRH and ICRH-SS schemes in blue and red respectively. Dashed lines correspond to the RF-power transferred on electrons. The total input power is 5.7MW. Integrating the total collisional power transferred to the background plasma by the Jacobian radial-volume factor $\sqrt{g}$ gives the total collisional power as 5.3MW and 5.1MW for ICRH and ICRH-SS respectively. Note that the ICRH case signficiantly over-estimates the collisional power transfer, as mode conversion effects were not included and would dominate RF-power absorption for ICRH (but not ICRH-SS), and almost all power would be transferred to the electrons. The ICRH case is presented in this figure purely to illustrate the differences in collisional heating power if the two cases received equal RF-power.

electron population through Coulomb collisions, as shown in figure 9. The collisional power density shown in figure 9 reflects the improvement in core power efficiency by using the ICRH-SS heating scheme over ICRH. The improvement comes almost entirely from the increase in power transferred to the electrons. This improvement in power transfer to the core background plasma can be explained by the improved RF-pinch effect from equation (34), which is also visible from figure 6.

Looking at figure 9 we observe a big difference between the ICRH-SS and ICRH curves in the plasma core ($r/a < 0.5$), but not at the periphery ($r/a > 0.5$) where red curves almost coincide with the blue ones. This fact represents an additional support our theory: according to equation (68), the ICRH-SS condition $\lambda_* < \lambda_{max}^{pas}$ is not satisfied at the periphery of discharge # 91256 and, therefore, in this region no big difference between discharge # 91256 and its modified version was expected. On the other hand, behaviour of fast ions in the periphery determines fast-ion losses. This explain why particle loss fractions are roughly the same in ICRH-SS and ICRH (6.22% and 5.86% , respectively, at t= 0.5s), their ratio is $6.22/5.86 = 1.06$. The ratio of energy losses is higher because lost particles have higher energy in the ICRH-SS

case, $10.08/6.72 = 1.5$. This is approximately the same as the ratio of the deposition power densities $P_{icrh-ss}/P_{icrh} = 1.44$ at $r/a = 0.1 - 0.2$, although total deposion powers were approximstely equal: $\mathcal{P}_{icrh}/\mathcal{P}_{icrh-ss} = 5.3/5.1 = 1.04$. This indicates that some accelerated ions diffused outwards.

6. Summary and discussion

Effects of shifting the QL separatrix to the region of passing particles are considered. The analysis is carried out for a tokamak magnetic configuration with $B = \bar{B}(1-\epsilon\cos\vartheta)$, where $\epsilon = r/R$, but it can be generalized to be valid for stellarators. The analysis is based on the 2-D and 3-D quasilinear equations for the ion distribution function, where the wave amplitude is a parameter. Therefore, our theory is not restricted to 3-ion scheme or any other scheme; it can be relevant to schemes employing fundamental cyclotron resonance and other harmonics as well.

The obtained results can be summarized as follows.

The QL separatrix ($\lambda = \lambda_l \equiv l\lambda_*$) in the space of $(\lambda, \mathcal{E}, r)$ is a kind of attractor, the ions approach it during acceleration caused by their interaction with RF waves through cyclotron resonance. This result is generic: it is valid for any particle orbits (including orbits crossing the magnetic axis) in any magnetic configuration; quasilinear routes do not depend on the magnitude of absorbed power. Approaching the separatrix, passing particles remain passing, whereas trapped particles may become passing during ICRH-SS (in contrast to particle behaviour during conventional ICRH). This difference between ICRH-SS and ICRH is clearly seen in figure 1. Although JET parameters were used, the picture on the left panel of this figure is similar to that shown for the Wendelstein 7-X stellarator in reference [2].

In tokamaks the magnitude of λ^{pas}_{max}, which represents a border between the regions of passing particles and trapped particles, depends on the radial coordinate, $\lambda^{pas}_{max} \approx 1-\epsilon$ for particles with standard orbits (i.e., for particles with $\Delta_b \ll r$, where Δ_b the orbit width). On the other hand, the ICRH-SS condition $\lambda_l < \lambda^{pas}_{max}$ is actually a restriction on the wave frequency, $\omega/\bar{\omega}_B > l(\lambda^{pas}_{max})^{-1}$. This restriction may be not satisfied in the plasma periphery because $(\lambda^{pas}_{max})^{-1}$ for standard orbits is a growing function of r, see right panel in figure 1. Then the radial motion of trapped particles along QL characteristics facilitates their orbit transformation into passing particles in the case when this motion is directed inwards (which takes place for negative toroidal mode numbers, $n < 0$), but it may prevent the transformation of particles moving outwards (when $n > 0$). The inward / outward motion is a positive / negative factor for passing particles, too. However, as shown in section 3.2, the radial displacement of passing particles is determined by the poloidal mode numbers (m). Due to this, it is much less than that of trapped particles for $m \ll n$ or when the m spectrum is symmetric, see e.g., figure 2. If so, QL characteristics of passing particles weakly depend on radius.

When the condition $\Delta_b \ll r$ is not satisfied, λ^{pas}_{max} depends not only on r but also on $\mathcal{E}$ and the sign of $v_\parallel$. In the limit case of particles with orbits crossing the magnetic

axis $\lambda_{max}^{pas} = 1 - \hat{s}^{2/3}$ when $v_{\|}(r = 0) < 0$ ($\hat{s} \sim q\rho/R_0$), but particles are passing or semi-passing (trapped poloidally) for $v_{\|} > 0$, see, e.g. [11]. ICRH-SS ensures that they remain passing, decreasing their λ value in comparison to ICRH, which makes the radial distribution of these ions more peaked.

Pitch-angle scattering produced by Coulomb collisions tends to minimize positive effects of ICRH-SS. Our estimates based on the comparison of the QL flux over λ and corresponding collisional flux indicate that the QL flux can dominate for realistic assumptions.

Numerical calculations have been made with the SCENIC code to compare conventional ICRH and ICRH-SS schemes. This is important to illustrate experimental feasibility of such heating scheme, and to provide detailed insight into the workings of the ICRH-SS scheme. The simulation of the ICRH-SS scheme ensured that the condition $\lambda_l < \lambda_{max}^{pas}$ was met, whereas the ICRH simulation applied heating with $\lambda_l > \lambda_{max}^{pas}$. The simulations were carried out for a JET plasma with combined ICRH and NBI heating. Plasma parameters were chosen to correspond to JET parameters to compare with the research of [3] and [4]. ICRH-SS simulations corresponded to these two articles, but an additional simulation of the conventional ICRH scheme applied the exact same plasma parameters but with a reduced RF-wave frequency of a factor of 1.19. The results confirm the previous theoretical conclusions that trapped particle fractions are reduced in the core region by applying ICRH-SS as opposed to ICRH. It was found that in the ICRH-SS case most accelerated ions had larger longitudinal velocities (smaller λ) and particle orbits were passing, whereas orbits had banana shape due to ICRH, as was predicted by our theory. The SCENIC simulations also illustrated that the QL flux beneficial for driving energetic passing particle populations dominated over the effects of Coulomb collisions. The numerical results show an increase in fast ion generation and core plasma heating performance using the ICRH-SS scheme. An increase in the RF-pinch effect for ICRH-SS was also reflected by the fast ion pressure, in addition to significantly larger concentrations of MeV range ions. The significant increase in energetic ions above the critical energy $\sim$ 110 keV for the ICRH-SS scheme leads to a larger fraction of the total collisional power transferred to electrons rather than the background ions.

Note that particle orbits shown in figure 6 (right panel) pass rather close to magnetic axis. Because of this, one could think that ion orbits before acceleration ($\mathcal{E} \leq 100$ keV) were non-standard. However, our simple estimates indicate that orbits of these particles were standard, although MeV particles had definitely non-standard orbits. The type of orbits is, however, of minor importance because, as was already emphasized, the QL routes do not depend on the orbit shape. Figure 8 (upper panel) clearly shows this: most of particles are located to the left of the separatrix, which is ~ 0.9 for ICRH-SS and ~ 1.07 for ICRH (the separatrix corresponds to infinite energy). On the other hand, banana orbits were produced by ICRH. Thus, the simulation convincingly has shown that the shifted separatrix and concomitant enlarged Doppler shift resulted in (i) the approach of the pitch parameter λ of accelerated ions to the separatrix in both cases,

independently on the orbit shape; (ii) the formation of trapped ions in the ICRH scheme but passing ions in the case of ICRH-SS. These results strongly support the developed theory.

Because of enlarged ratio of $\omega/\bar{\omega}_B$ in ICRH-SS, the frequency Doppler shift of resonant particles should exceed a certain value. For given ratio $\omega/\bar{\omega}_B$, this imposes a requirement on the product $k_\parallel\rho_\parallel$ of the particles, which should be as large as $k_\parallel\rho_\parallel = \tilde{\omega} - l(1+\epsilon)$, being minimum at the high-field side of flux surface. This means that, generally speaking, antennas producing waves with larger longitudinal wavenumbers than those in convention ICRH are required, which may be a disadvantage of ICRH-SS because it somewhat increases the evanescence region. On the other hand, available antennas designed for ICRH can be suitable for ICRH-SS in the plasma core (where λ_{max}^{pas} is minimum), at least, when the $l = 1$ resonance is employed. Moreover, they can be suitable at the periphery, too, provided that the ion energy is sufficiently large. In the case of the QL separatrix located at the border between regions of passing particles and trapped particles, $\lambda_l = \lambda_{max}^{pas}$, the restriction on minimum $k_\parallel\rho_\parallel$ is weak in the region close to this border.

The ICRH-SS can be realized in different scenarios. Below we briefly discuss this issue.

As known, the quasilinear diffusion coefficient contains terms proportional to $|E_+|^2 J_{l-1}^2(z)$ and $|E_-|^2 J_{l+1}^2(z)$, with $z = k_\perp\rho_\perp$. It follows from here that, due to $J_{l-1}^2 \approx 1$ for $l = 1$ and $0 \le z \lesssim 1$, the $l = 1$ resonance is most attractive provided that the electric field rotating in the ion direction, E_+, is considerable. This implies that the $l = 1$ resonance will work when the gyrofrequency of fast ions exceeds that of thermal ions and the fast ion population is so small that it has a negligible influence on the wave polarization. For instance, it will work in a deuterium plasma containing a small number of fast protons which are in resonance with the RF field ($\omega \approx \omega_B^{(H)}$): then $\omega \approx 2\omega_B^{(D)}$ and, therefore, $E_+/E_- \approx 1/3$ [21], being determined by the bulk plasma. It is clear that the wave has this polarization also when the system plasma - beam contains only one ion species (for instance, thermal deuterons and fast deuterons). Then the wave with $\omega \approx 2\omega_B^{(D)}$ can be in the $l = 2$ resonance with fast ions, but z should be not very small to provide acceptable J_{l-1}^2. The $l = 2$ resonance works also in a D-T mixture. These methods are widely used in current and planned experiments with ICRH. In particular, concerning experiments on JET where these schemes of ICRH were used see, e.g., [22, 23].

In a plasma with a moderate number of minority ions whose gyrofrequency differs from that of the majority ions an important role may belong to the ion-ion hybrid resonance and mode conversion (MC) layer where the ratio of E_+/E_- is very large, see e.g., overview [24] and [25]. This opens a possibility of strong wave-particle interaction provided that there are resonant particles in the MC layer [15]. Due to large E_+, these ions can be strongly accelerated but their number is very small because of small region where MC layer is located. Nevertheless, the neutron yield due to D-D fusion reaction in a plasma with the ion temperature about a few keV should strongly grow because in

this case the beam-plasma reaction dominates and strongly increases due to acceleration of beam particles (especially, when thermal D-ions are in minority but thermal H-ions are in majority). The 3-ion ICRF experiments in H-D plasmas using fast NBI ions as resonant absorbers at the IIH layer showed a strong enhancement of neutron rate in the combined phase with ICRF and NBI heating [3].

On the other hand, the effect of strong acceleration on the neutron yield of D-T reaction in a plasma with $T \sim 10$ keV would be relatively small. Scenarios providing a moderate acceleration of fast ions in a wide plasma region (rather than in a narrow layer) should be employed in D-T plasmas when the aim of RF heating is to increase the fusion reaction rate and energy gain.

In conclusion we note that the most attractive application of ICRH-SS in stellarators, such as Wendelstein 7-X and a Helias reactor could be the use it for the transformation of transitioning fast ions to passing ones: transitioning fast particles undergo stochastic (collisionless) diffusion and can be lost in optimized quasi-isodynamic stellarators [26, 27]. These particles are located mainly at $r/a > 0.3$ in Wendelstein-type machines. Therefore, schemes with radially peaked heating can hardly affect transitioning particles, but they can produce strongly accelerated passing fast ions, as shown for W7-X in [4]. For transitioning-to-passing conversion in W7-X, RF energy should be deposited at $r/a > 0.3$ and the magnetic field should be decreased somewhat below its standard value (at least, in the high mirror configuration) [2]. The latter requirement comes from the resonance condition because of relatively small longitudinal velocities of transitioning particles.

Acknowledgments

Two authors (YK and HP) would like to thank Per Helander for discussions at IPP, which eventually resulted in fulfillment this work. Two authors (YK and VL) thank Henri Weisen for a discussion on ICRH-SS at JET.

This work was carried out within the framework of the EUROfusion Consortium and received funding from the EURATOM research and training programme 2014–2018 and 2019-2020 under grant agreement No. 633053. The views and opinions expressed herein do not necessarily reflect those of the European Commission. The work was also supported by the STCU-NASU Project No. 6392.

The work was also supported in part by the Swiss National Science Foundation. The Piz Daint (CSCS, Switzerland) and the MARCONI-Fusion (CINECA/ENEA, Italy) supercomputer facilities were used for the simulations presented in this research. Numerical calculations using Piz Daint were supported by a grant from CSCS under project ID's "s914" and "s821".

References

[1] Goldston R J, White R B and Boozer A H 1981 *Phys. Rev. Lett.* **47** 647

[2] Kolesnichenko Ya I, Lutsenko V V, Rudenko T S, and Helander P 2017 *Nucl. Fusion* **57** 066004
[3] Ongena J *et al* 2017 *EPJ Web. Conf.* **157** 02006
[4] Patten H W, Graves J P, Cooper W A, Eriksson J, Pfefferle V, W7-X team and JET contributors 2020 *Phys. Rev. Lett.* **124** 155001
[5] Jucker M *et al* 2011 *Comp. Phys. Comm.* **182** 912
[6] Lerche E, Van Eester D, Krasilnikov A, Ongena J, Lamalle P and JET-EFDA contributors 2009 *Plasma Phys. Control. Fusion* **51** 044006
[7] Krasilnikov A. V.,Van Eester D., Lerche E. *et al* 2009 *Plasma Phys. Control. Fusion* **51** 044005
[8] Stix T H 1992 *Waves in Plasmas* (New York: Springer-Verlag)
[9] Kolesnichenko Ya I, Lutsenko V V, Rudenko T S 2018 *Ukrainian Journal of Physics* **63** 232
[10] Belikov V S, Kolesnichenko Ya I 1994 *Plasma Phys. Control. Fusion* **5** 1703
[11] Kolesnichenko Ya I, Parail V V, Pereversev G V 1992 *Reviews of Plasma Physics* (N.Y.-London: Consultant Bureau) pp 1-192
[12] Eriksson L-G , Mantsinen M J, Borba D *et al* 1998 *Phys. Rev. Lett.* **81** 1231
[13] Hellsten T *et al* 2004 *Nucl. Fusion* **44** 892
[14] Kazakov Ye *et al* 2020 *Nucl. Fusion*, in press; https://doi.org/10.1088/1741-4326/ab9256
[15] Kazakov Ye, Van Eester D, Dumont R and J. Ongena J 2015 *Nucl. Fusion* **55** 032001
[16] Mellet N *et al* 2011 *Comp. Phys. Comm.* **182** 570
[17] Brambilla M 1999 *Plasma Phys. Control. Fusion* **41** 1
[18] Kirov K *et al 'Synergistic ICRH and NBI Heating for Fast Ion Generation and Maximising Fusion Rate in Mixed Plasmas at JET'*, 23rd Topical conference on RF-Power in Plasmas, Maz 14-17, 2019, Hefei, China
[19] Patten H *et al* 2018 *Plasma Phys. Contr. Fusion* **60** 085009
[20] Patten H, Development and optimisation of advanced auxiliary ion heating schemes for 3D fusion plasma devices. PhD thesis 9167, École Polytechnique Fédérale de Lausanne, 2019.
[21] Stix T H 1975 *Nucl. Fusion* **15** 737
[22] Start D F H, Jacquinot J, Bergeaud V *et al* 1998 *Phys. Rev. Lett.* **80** 4681
[23] Mantsinen M J, Eriksson L-G, Bhatnagar V P *et al* 1999 *Plasma Phys. Contr. Fusion* **41** 843
[24] Wesson J *et al* 2004 *Tokamaks* (Oxford: Clarendon Press, Third Edition)
[25] Mayoral M-L, Lamalle P U, Van Eester D *et al* 2006 *Nucl. Fusion* **46** S550
[26] Tykhyy A V 2018 *Ukrainian Journal of Physics* **63** 495
[27] Beidler C D, Kolesnichenko Ya I, Marchenko V S, Sidorenko I N and Wobig H 2001 *Phys. Plasmas* **8** 2731